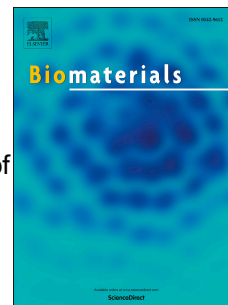


Journal Pre-proof

Dual-stimuli responsive nanotheranostics for mild hyperthermia enhanced inhibition of Wnt/ β -catenin signaling

Tao Feng, Liang Zhou, Zhongyuan Wang, Chunxiao Li, Yifan Zhang, Jing Lin, Desheng Lu, Peng Huang



PII: S0142-9612(19)30827-0

DOI: <https://doi.org/10.1016/j.biomaterials.2019.119709>

Reference: JBMT 119709

To appear in: *Biomaterials*

Received Date: 29 January 2019

Revised Date: 4 December 2019

Accepted Date: 18 December 2019

Please cite this article as: Feng T, Zhou L, Wang Z, Li C, Zhang Y, Lin J, Lu D, Huang P, Dual-stimuli responsive nanotheranostics for mild hyperthermia enhanced inhibition of Wnt/ β -catenin signaling, *Biomaterials* (2020), doi: <https://doi.org/10.1016/j.biomaterials.2019.119709>.

This is a PDF file of an article that has undergone enhancements after acceptance, such as the addition of a cover page and metadata, and formatting for readability, but it is not yet the definitive version of record. This version will undergo additional copyediting, typesetting and review before it is published in its final form, but we are providing this version to give early visibility of the article. Please note that, during the production process, errors may be discovered which could affect the content, and all legal disclaimers that apply to the journal pertain.

© 2019 Published by Elsevier Ltd.

Dual-Stimuli Responsive Nanotheranostics for Mild Hyperthermia Enhanced Inhibition of Wnt/ β -Catenin Signaling

Tao Feng,^{1,#} Liang Zhou,^{2,#} Zhongyuan Wang,^{2,#} Chunxiao Li,¹ Yifan Zhang,¹ Jing Lin,^{1,*} Desheng Lu,^{2,*} Peng Huang^{1,*}

¹Marshall Laboratory of Biomedical Engineering, International Cancer Center, Laboratory of Evolutionary Theranostics, School of Biomedical Engineering, Shenzhen University Health Science Center, Shenzhen, 518060, China

²Guangdong Key Laboratory for Genome Stability & Disease Prevention, International Cancer Center, Department of Pharmacology, Shenzhen University Health Science Center, Shenzhen 518060, China

Co-first author

Corresponding authors:

Prof. Jing Lin, E-mail: jlin@szu.edu.cn;

Prof. Peng Huang, E-mail: peng.huang@szu.edu.cn;

Prof. Desheng Lu, E-mail: delu@szu.edu.cn.

Keywords: Nanotheranostics, melanin coated magnetic nanoparticles, obatoclax, mild hyperthermia, Wnt/ β -catenin signaling pathway.

Abstract

Wnt/ β -catenin signaling cascade is highly associated with tumorigenesis and progression of various cancers. Targeting Wnt/ β -catenin signaling exhibits a promising way for cancer treatment. Herein, dual-stimuli responsive nanotheranostics was synthesized, which was composed of melanin coated magnetic nanoparticles (MMNs) and Wnt signaling inhibitor obatoclax (OBX) for multimodality imaging guided mild hyperthermia-enhanced chemotherapy. The MMNs could be used as contrast agents for magnetic resonance imaging

(MRI) and photoacoustic imaging (PAI) guided photothermal therapy. In addition, OBX-loaded MMNs (OBX-MMNs) were specific response to both pH changes and near-infrared (NIR) light illumination, which could trigger OBX release. Most intriguingly, tumor tissue accumulation and cellular internalization of this nanotheranostics could be dramatically enhanced through mild hyperthermia generated by laser-irradiated MMNs. Laser irradiation exhibited efficient chemotherapeutic outcome through enhancing OBX-mediated inhibition of the Wnt/ β -catenin signaling. Our results indicated the as-prepared OBX-MMNs hold great potential for MR/PA dual-modal imaging guided mild hyperthermia-enhanced chemotherapy.

Introduction

Wnt/ β -catenin signaling as a crucial pathway regulates a wide range of physiological processes, including embryonic development, cell proliferation and migration, and cell fate specification [1-3]. Dysregulation of Wnt/ β -catenin signaling could induce development and progression of a variety of cancers, including of breast cancer and colorectal cancer [4-7]. Therefore, the critical roles of Wnt/ β -catenin signaling pathway in cancers make it a promising target for pharmacological research [1, 8, 9]. Currently, attempts have been made for therapeutic intervention of the Wnt signaling pathway regarding the tumor inhibition [10]. Recently, the antitumor compound obatoclax (OBX) was used for a novel Wnt/ β -catenin signaling inhibitor [4-6]. How to enhance OBX-mediated inhibition efficiency of Wnt/ β -catenin signaling is a tough challenge.

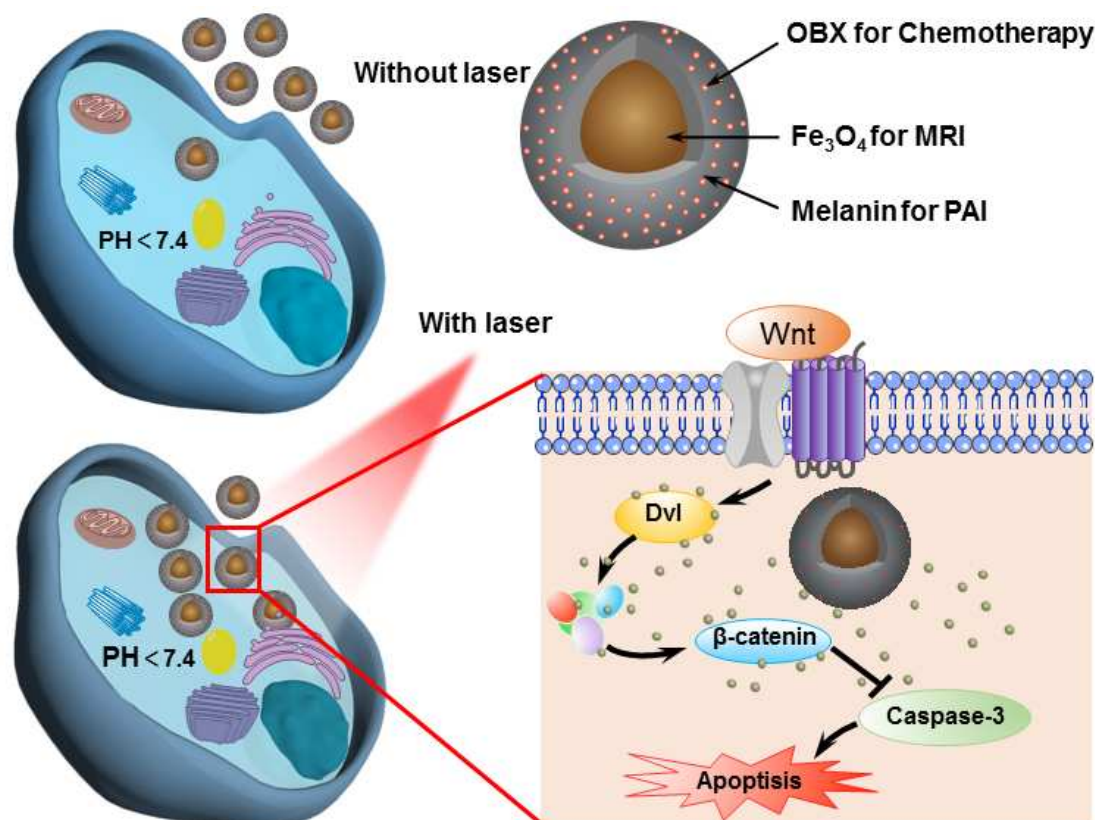
Although several types of inhibitors have been developed and presented potent efficacy in cancer treatment, the intrinsic drawback of chemotherapeutics in damaging normal cells cannot be avoided [11-16]. One possible solution is the delivery of chemotherapeutic drugs by nanocarriers to achieve the enhanced and selective accumulation of drugs at the tumor location *via* the enhanced permeability and retention (EPR) effect [15, 17-24].

Moreover, additional benefits of nanocarriers include the prolong half-life of drugs in circulation and the controllable release kinetics [25, 26]. Till now, many nanocarriers have not only been effectively delivered at tumor sites, but their inherent physical properties have also made them promising theranostic agents [27-30].

Recently, mild hyperthermia (39~42°C) has been employed to increase the permeability of cell membrane and blood vessels, thus improving the cellular uptake and therapeutic efficacy of chemotherapeutic drugs [31-33]. To date, many kinds of photothermal agents for hyperthermia (e.g. gold nanoshells, copper sulfide, black phosphorus (BP)) have been prepared [34-38]. For example, Lu *et al.* explored copper sulfide doped periodic mesoporous organosilica nanoparticles loaded with doxorubicin for mild hyperthermia-enhanced chemotherapy [31]. Wang *et al.* reported paclitaxel-loaded human modified BP for mild hyperthermia-enhanced chemotherapy and chemo-photothermal combination therapy [39]. Among these photo-activated nanomaterials, melanin, as a natural bio-pigment existing in the human body, stands out not only for its good biodegradability and biocompatibility, but also for its strong absorbance in the near-infrared (NIR) region, promising for photoacoustic imaging (PAI) and photothermal therapy (PTT) [40-43]. Based on these properties, melanin coated magnetic nanoparticles (MMNs) were designed and synthesized for multimodal imaging guided PTT [40, 41, 44, 45].

In this study, we developed a multifunctional nanoplatform, which was composed of MMNs and the Wnt signaling inhibitor obatoclox (OBX), denoted as OBX-MMNs, for magnetic resonance imaging (MRI) and PAI guided mild hyperthermia-enhanced chemotherapy (**Scheme 1**). MMNs were prepared by one-pot biomimetic synthesis method [46]. OBX was loaded into MMNs *via* π - π stacking and hydrophobic interaction. OBX-MMNs have the following features: i) MR/PA dual-modal imaging of MMNs holds more accurate diagnosis and imaging than single mode; ii) MMNs could generate

hyperthermia upon laser irradiation to increase the accumulation of OBX in tumor cells/tissues; iii) pH-/NIR-induced drug release can greatly improve the therapeutic effect while reducing side effects on healthy tissues [21, 47]. More intriguingly, detailed studies revealed that mouse mammary tumor virus (MMTV)-Wnt1 transgenic tumor could be effectively suppressed by blocking the Wnt signaling pathway.



Scheme 1. Schematic illustration of the OBX loaded MMNs (OBX-MMNs) for PA/MR multimodality imaging guided mild hyperthermia-enhanced chemotherapy, through enhancing OBX-mediated inhibition of the Wnt/ β -catenin signaling pathway.

Results and Discussions

Preparation and Characterization of OBX-MMNs.

Biomimetic synthesis method was used to prepare MMNs through the

co-precipitation of melanin with Fe^{3+} and Fe^{2+} ions (molar ratio 2:1) under nitrogen protection and alkaline conditions. As shown in Fig. 1a, transmission electron microscopy (TEM) image indicated MMNs are spherical with 15 nm in diameter. OBX was loaded into MMNs *via* π - π stacking and hydrophobic interaction. OBX-MMNs showed the absorption peak of OBX at 540 nm, suggesting the OBX was successfully loaded (Fig. 1b and Fig. S1a, Supporting information). The color of MMNs aqueous solution was changed from black to brownish black after OBX loading (Fig. S1b). The maximal loading efficiency of OBX was determined around 40%, demonstrating high loading capability of MMNs (Fig. S2a). To evaluate the photothermal property of OBX-MMNs, different concentrations of OBX-MMNs solutions were exposed to an 808 nm laser (5 min, 1.0 W cm^{-2}). As shown in Fig. S2b-c, the temperature of solutions displayed an OBX-MMNs concentration-dependent increase. Even at the low concentration of MMNs (equivalent OBX dose: $120 \mu\text{M}$), the temperature of OBX-MMNs solution still increased rapidly, and the temperature change (ΔT) was $27.3 \text{ }^\circ\text{C}$ within 5 min. The temperature change of OBX-MMNs solution was monitored by several on-off cycles of laser irradiation to evaluate the photothermal stability. As indicated by Fig. S2d, the temperature could rise to the same level even after six cycles, suggesting the good photothermal stability of MMNs.

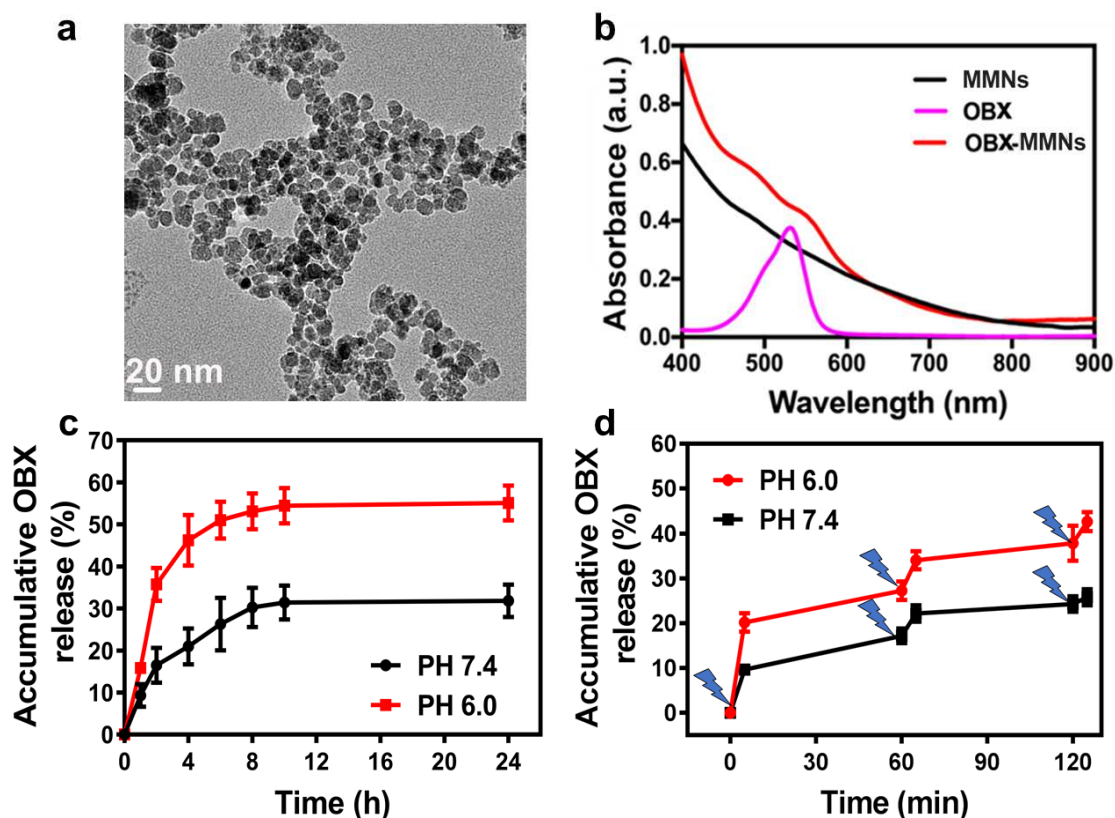


Fig. 1. (a) TEM image of MMNs. (b) UV-Vis-NIR absorption spectra of OBX, MMNs and OBX-MMNs aqueous solutions. (c) OBX release profiles of OBX-MMNs from OBX-MMNs at different pH values. (d) OBX release profiles from OBX-MMNs at different pH values with an 808 nm laser (5 min, 1.0 W cm⁻²) irradiation (equivalent OBX dose:120 μ M). All data are expressed as mean \pm SD (n = 3).

Next, to verify pH-responsive feature of OBX-MMNs, the released amount of OBX from OBX-MMNs was monitored under different pH conditions. At pH 7.4, OBX-MMNs could generally maintain its stability with \sim 32% OBX released after 24 h incubation. However, about 51% cumulative release was observed under the condition of pH 6.0, which is contributed to the enhanced hydrophilicity of protonated OBX (Fig. 1c). In addition to pH, mild hyperthermia was reported to accelerate the drug release [31]. Thus, the OBX release upon laser irradiation was also investigated. As shown in Fig. 1d, laser irradiation could promote the OBX release to some extent at pH7.4 while significantly

enhanced after laser irradiation at pH 6.0. After three cycles of laser irradiation, the release percentage of OBX at pH 6.0 reached around 43% within 2 h, which was much higher than pH7.4 group (25%), and higher than 35.7% at pH 6.0 but without laser irradiation. Therefore, the OBX released from OBX-MMNs could be triggered by both pH changes and light illumination.

Cellular Uptake and Cytotoxicity *in Vitro*.

To explore *in vitro* hyperthermia effect, we investigated the cellular uptake of OBX on MDA-MB-231 and MDA-MB-468 human breast cancer cells respectively. Compared to free OBX group, cells incubated with OBX-MMNs displayed higher fluorescence intensity (Fig.S3a-b). Then we investigated the cellular uptake of free OBX and OBX-MMNs in the condition of with or without NIR laser irradiation. In the OBX-MMNs group without laser irradiation, OBX was released from OBX-MMNs in the intracellular acidic environment, resulting in red fluorescence signals in the cytoplasm (Fig.2a and Fig. S4a). After 5 min laser irradiation, stronger red fluorescence signals of OBX were observed in the cytoplasm. Subsequently, FACS analysis was used to quantify fluorescence intensities of intracellular OBX. In MDA-MB-231 cells, it was observed that the fluorescence intensities of OBX-MMNs treated cells plus laser irradiation was 1.7 times stronger than OBX-MMNs treated cells and 2.7 times stronger than free OBX treated cells (Fig. 2b-c and Fig. S4b-c). These results consolidated that mild hyperthermia could promote the cellular internalization of OBX-MMNs.

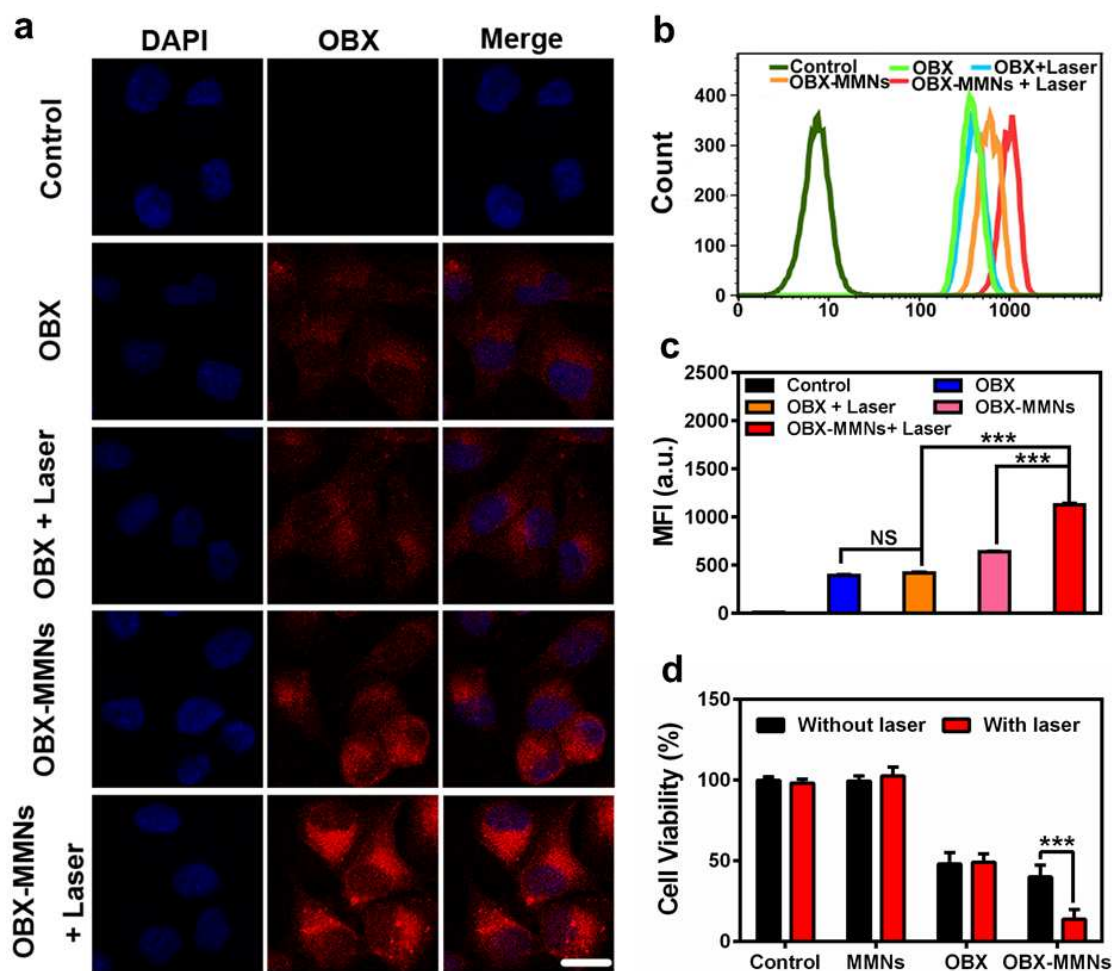


Fig. 2. (a) Confocal laser scanning microscopy (CLSM) images of MDA-MB-231 cells incubated with free OBX or OBX-MMNs (equivalent OBX dose: 500 nM) with/without an 808 nm laser (5 min, 1.0 W cm⁻²). (b) Flow cytometry analyses and (c) corresponding mean fluorescence intensity (MFI) of MDA-MB-231 cells incubated with free OBX or OBX-MMNs (equivalent OBX dose: 500 nM) with/without an 808 nm laser (5 min, 1.0 W cm⁻²). (d) Relative MDA-MB-231 cells viability incubated with free OBX or OBX-MMNs (equivalent OBX dose: 1000 nM) with or without an 808 nm laser (5 min, 1.0 W cm⁻²). All data are expressed as mean \pm SD (n = 5). NS: not significant, ****P* < 0.001.

The cell cytotoxicity of OBX-MMNs was then evaluated by MTT assay. The MMNs only caused negligible toxicity to both MDA-MB-231 and MDA-MB-468

cells after 24 h incubation even at a high concentration (equivalent OBX dose: 5000 nM L⁻¹). After OBX loading, the effect of chemotherapy was increased with the concentration of OBX, and stronger than that of free OBX group (Fig. S5). Upon 808 nm laser irradiation (1.0 W cm⁻², 5 min), the cell viability of MMNs group did not change, indicating that mild hyperthermia did not kill cells, whereas the cell viability of OBX-MMNs with laser group was lower than OBX (Fig. 2d and Fig. S4d). These results illustrated that mild hyperthermia could remarkably strengthen the chemotherapeutic effect of OBX-MMNs, while no obvious photothermal therapeutic effect due to the limited increase of temperature.

Wnt/ β -Catenin Signaling Inhibition in Breast Cancer Cells.

The transcriptional coactivator β -catenin is a core component of the Wnt signaling pathway and its activity is tightly controlled by degradation complexes that phosphorylate β -catenin by casein kinase 1 (CK1) and GSK3 β , resulting in β -catenin degradation *via* the ubiquitination-proteasome pathway. Upon Wnt stimulation, β -catenin rapidly gathered in the cytoplasm and entered the nucleus, then interacted with the TCF/LEF transcription factor, thus activating transcription of the Wnt target genes. Then we assessed the effect of OBX-MMNs on Wnt/ β -catenin signaling in two breast cancer cell lines: MDA-MB-231 and MDA-MB-468, respectively. As shown in Fig. 3a-c and Fig. S6-8, both free OBX and OBX-MMNs with/without laser irradiation could efficiently decrease the protein levels of phosphorylated LRP6 (Ser1490), total LRP6, phosphorylated DVL2 (upper band), phosphorylated GSK3 β (Ser9), active and total β -catenin. Moreover, the treatment also increased the expression of cleaved caspase-3, which suggested the inducing apoptosis by both free OBX and OBX-MMNs with/without laser irradiation (Fig. S9). However, OBX-MMNs plus laser irradiation had an enhanced inhibitory effect

due to the higher cellular uptake, closely followed by OBX-MMNs. Laser irradiation only did not promote the inhibitory capability of free OBX. These results indicated that mild hyperthermia mediated by MMNs upon laser irradiation could efficiently induce the apoptotic effect, thus further inhibiting the Wnt/ β -catenin signaling cascade.

Obatoclox is a well-known Bcl2 inhibitor^[48]. In order to validate the importance of Wnt and Bcl2 signaling in the anticancer activity of obatoclox, we knocked down β -catenin (Fig. S10a) or Bcl2 (Fig. S10b) using lentivirus-mediated shRNA in MDA-MB-231 and MDA-MB-468 cells. Our results showed that the inhibitory effect of obatoclox on cell viability could be rescued by either β -catenin or Bcl2 knockdown (Fig. S10c-d), while the inhibitory effect of Bcl2 specific inhibitor ABT199 on cell viability was reversed by Bcl2 knockdown, but not by β -catenin knockdown (Fig. S10e-f). Western blot results revealed that obatoclox could still reduce the protein levels of phosphorylated LRP6 (Ser1490), total LRP6, phosphorylated DVL2 (upper band), phosphorylated GSK3 β (Ser9), active and total β -catenin after Bcl2 knockdown in MDA-MB-231 and MDA-MB-468 cells (Fig. S10g-h). Furthermore, obatoclox had little effects on the expression of Wnt target genes cyclin D, LEF1 and fibronectin after β -catenin knockdown (Fig. S10i-j). In addition, the MDA-MB-231 or MDA-MB-468 cells were treated with Wnt3A conditioned medium (Wnt3ACM) to activate the Wnt signaling pathway. As expected, Wnt3ACM treatment markedly increased the mRNA level of Wnt target genes, and obatoclox strongly repressed the Wnt3A-induced expression of Wnt target genes (Fig. S10k-m). These results indicated that obatoclox exerted its biological effect through targeting Wnt and Bcl2 signaling.

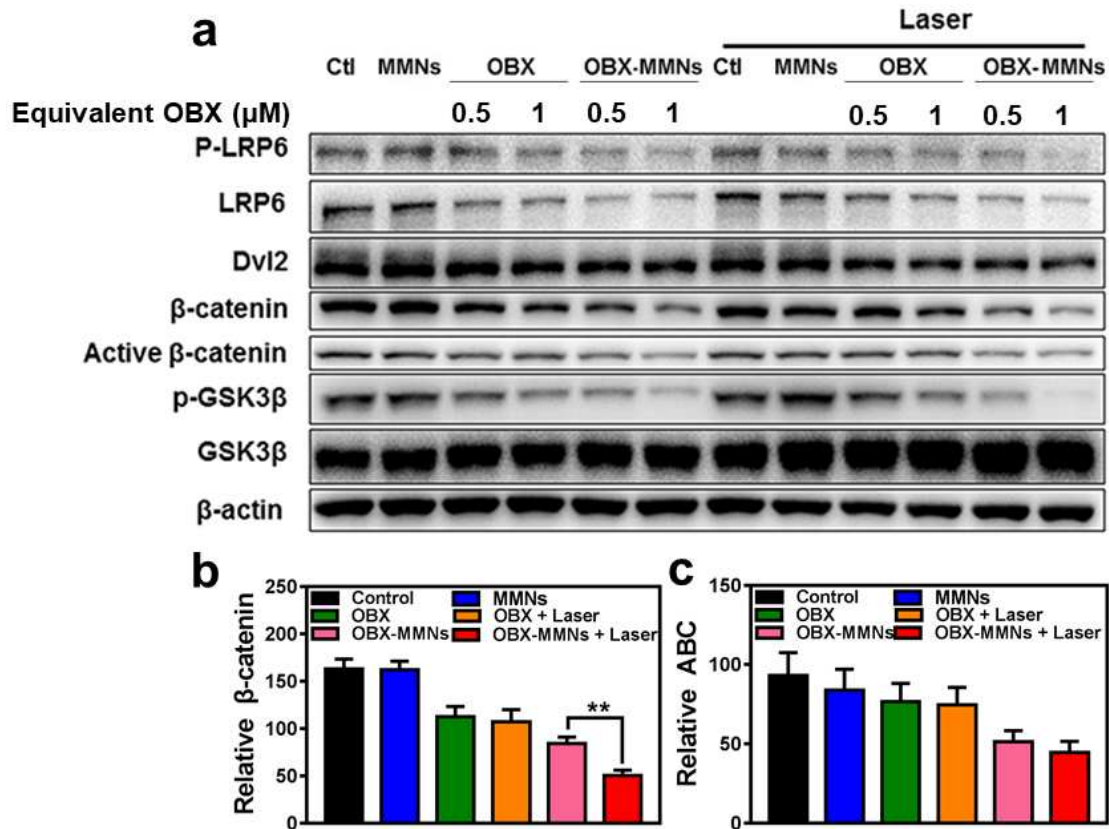


Fig. 3. OBX-MMNs inhibits the Wnt/β-catenin signaling pathway in MDA-MB-231 cells. (a) Phosphorylated LRP6 (Ser1490), total LRP6, DVL2, phosphorylated GSK3β (Ser9), total GSK3β, active β-catenin, and total β-catenin in MDA-MB-231 cells incubated with free OBX or OBX-MMNs without or with an 808 nm laser (5 min, 1.0 W cm⁻²) were detected by immunoblotting. Among them, in the DVL band, upper band represents phosphorylated DVL2. (b) The corresponding expression levels of total β-catenin and (c) active β-catenin (ABC) in MDA-MB-231 cells incubated with free OBX or OBX-MMNs without or with an 808 nm laser (5 min, 1.0 W cm⁻²). All data are expressed as mean ± SD (n = 5). NS: not significant, ** P < 0.01.

***In vitro* and *in vivo* multimodal imaging of OBX-MMNs.**

The multimodal imaging capacity of OBX-MMNs was studied both *in vitro* and *in vivo*. As shown in Fig. 4a-b, the PA intensity of OBX-MMNs was linearly correlated with the concentration of OBX-MMNs. The PA signals of tumor tissues gradually augmented and peaked at 24 h, demonstrating high tumor

accumulation of OBX-MMNs (Fig. 4c-d). After mild hyperthermia treatment, the PA signals of tumor tissues were increased from 0.59 to 0.88, suggesting the enhanced tumor accumulation of OBX-MMNs. The T_2 -weighted MR signals of OBX-MMNs exhibited a negative correlation with concentrations (Fig. 4e). After intratumoral injection of OBX-MMNs, it can be clearly observed that the tumor tissue area is darkened (Fig. S11a-b). As shown in Fig. 4f, tumor tissues also had a strong darkness at 24 h post-injection, which decreased to 70.9% compared with 0 h (Fig. 4g). After mild hyperthermia treatment, the MR signals further decreased to 46.2%. These results demonstrated that OBX-MMNs have excellent PA/MR imaging capability and mild hyperthermia can improve the tumor accumulation of OBX-MMNs.

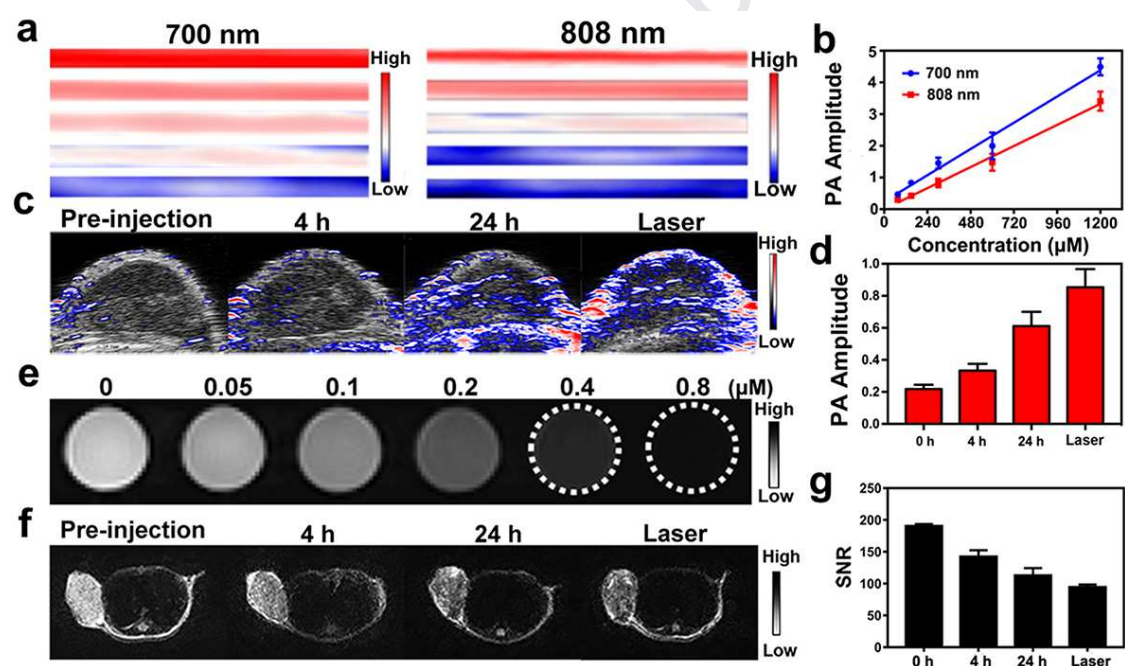


Fig. 4. *In vitro* and *in vivo* multimodal imaging. (a) PA images and (b) the corresponding PA amplitude of OBX-MMNs with different concentrations under 700 and 808 nm excitation, respectively. (c) PA images and (d) the relatively PA amplitudes at tumor sites of xenograft model of MMTV-Wnt1-derived tumors pre- and post-intravenous injection of OBX-MMNs under 808 nm excitation. (e) T_2 -weighted MR images of OBX-MMNs with different concentrations. (f) T_2 -weighted MR images and (g) the corresponding signal-to-noise ratios (SNR) of xenograft model of MMTV-Wnt1-derived tumors

pre- and post-intravenous injection of OBX-MMNs. All data are expressed as mean \pm SD (n = 3)

Antitumor Activity in Wnt1 Transgenic Mouse.

Finally, the chemotherapeutic effects of OBX-MMNs were evaluated in xenograft model of MMTV-Wnt1-derived breast tumors. First, *in vivo* tumor temperature changes of mice treated with PBS or OBX-MMNs were monitored by an infrared (IR) thermal camera. As shown in Fig. 5a-b, the temperature of tumor tissues was maintained at 40-42 °C during the 20 min laser irradiation in OBX-MMNs group while PBS group showed a negligible rise. Complete tumor elimination was achieved in the OBX-MMNs plus Laser group, the OBX-MMNs group showed a moderate tumor inhibition, but more efficient than free OBX group (Fig. 5c and Fig. S12). For OBX-MMNs plus laser group, both the tumor growth rate and tumor size were significantly suppressed, 80% mice exhibited a obviously longer survival span (> 42 days) than other four groups (Fig. 5d). Hematoxylin & eosin (H&E) staining of tumors with different treatments showed reduction in proliferation while increased the apoptosis of tumor cells, which further confirmed the improved therapeutic effect (Fig. 5e). Additionally, H&E staining images of major organs from all groups validated good biocompatibility of MMNs (Fig. S13). To confirm the change of Wnt signaling pathway in tumor tissues, we built another batch of same animal model, and the same way of administration, mice were uniformly sacrificed on the 18th day. As shown in Fig. S14a, treatments with free OBX, OBX-MMNs, or OBX-MMNs plus laser irradiation all reduced the tumor weight, with OBX-MMNs plus laser irradiation having the best effect. Meanwhile, the systemic toxicity of OBX-MMNs was investigated by the measurement of mouse body weight change. As shown in Fig. S14b, all treatments did not reduce the body weight of mice. The acute toxicity of OBX-MMNs was investigated by blood biochemical analysis. Compared with the control group, main parameters (serum glutamic-pyruvic transaminase (ALT), glutamic oxalacetic

transaminase (AST), creatinine (CREA) and blood urea nitrogen (BUN)) in healthy mice treated with OBX-MMNs were normal (Fig. S15), suggesting that no influence of OBX-MMNs on blood chemistry or functions of the liver and kidney in the treated mice. These results indicated that OBX-MMNs have good biocompatibility.

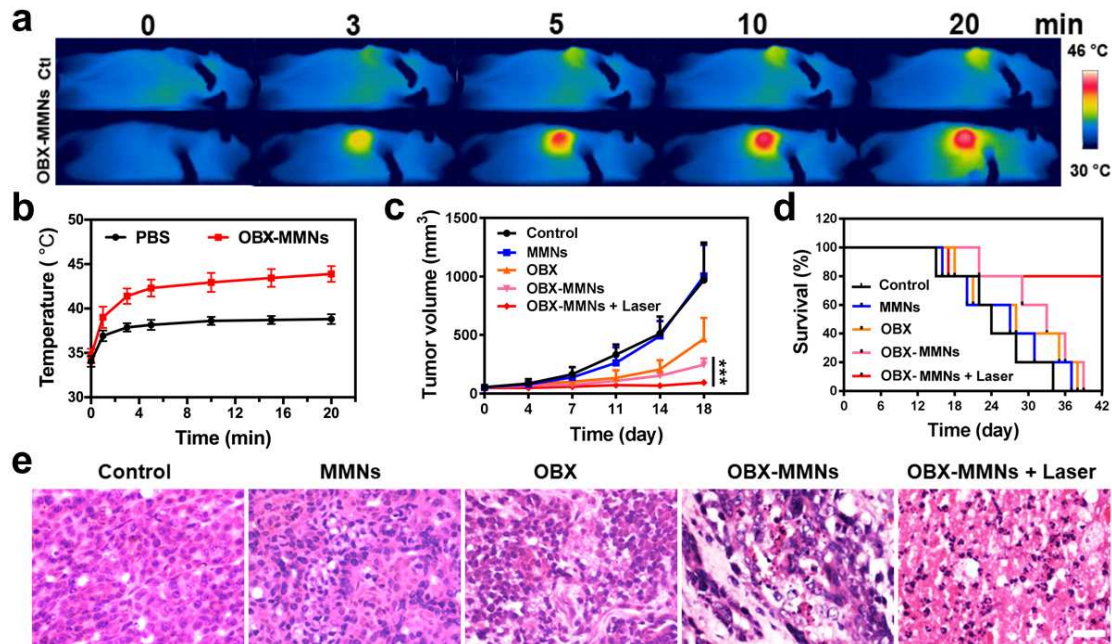


Fig. 5. *In vivo* anti-tumor effects of OBX-MMNs on xenograft model of MMTV-Wnt1-derived tumors. (a) Photothermal images of tumor-bearing mice injected with PBS or OBX-MMNs upon exposure to 20 min laser stimulation. (b) Relative temperature changes of tumor regions. (c) Tumor growth curve and (d) survival curves of tumor-bearing mice in different groups. (e) Hematoxylin & eosin (H&E) staining images of tumor tissues from different groups at day 18. Scale bar = 100 μ m. All data are expressed as mean \pm SD (n = 5). NS: not significant, *** $P < 0.001$.

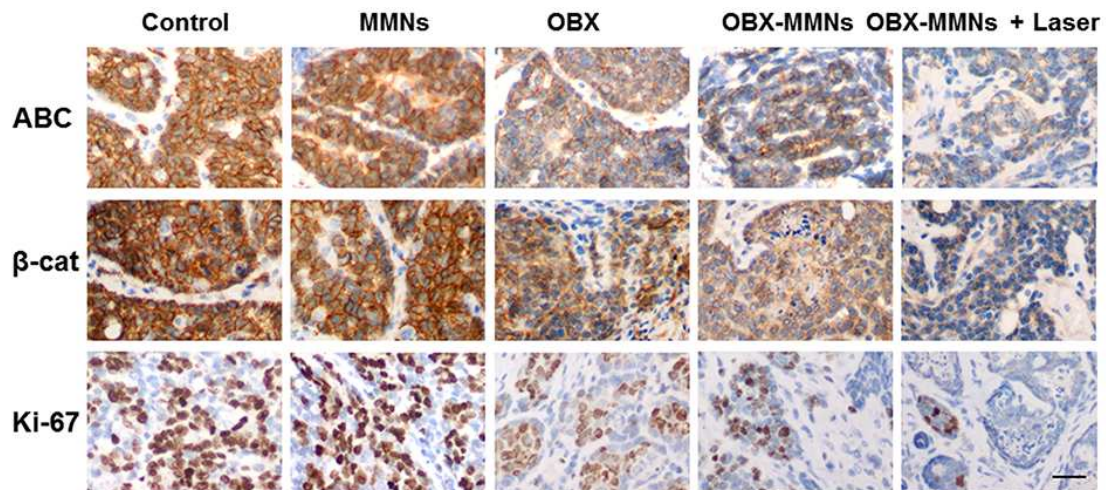


Fig. 6. Immunohistochemistry (IHC) shows OBX-MMNs significantly decrease proliferation marker and key factor in Wnt/ β -catenin signaling.

IHC of ABC, β -catenin and Ki-67. Scale bar: 100 μ m.

. As shown in Fig. 6, immunohistochemical staining images confirmed that OBX-MMNs plus laser treatment reduced the expression of Ki-67, ABC and total β -catenin in xenograft mice. In addition, compared with other groups, OBX-MMNs plus laser irradiation obviously reduced protein levels of phospho-LRP6 (Ser1490), total LRP6, phosphorylated and unphosphorylated DVL2, phospho-GSK3 β (Ser9), ABC and total β -catenin (Fig. 7a-c and S16). These results indicated that OBX-MMNs plus laser irradiation exhibited efficient chemotherapeutic outcome through enhancing OBX-mediated inhibition of the Wnt/ β -catenin signaling pathway.

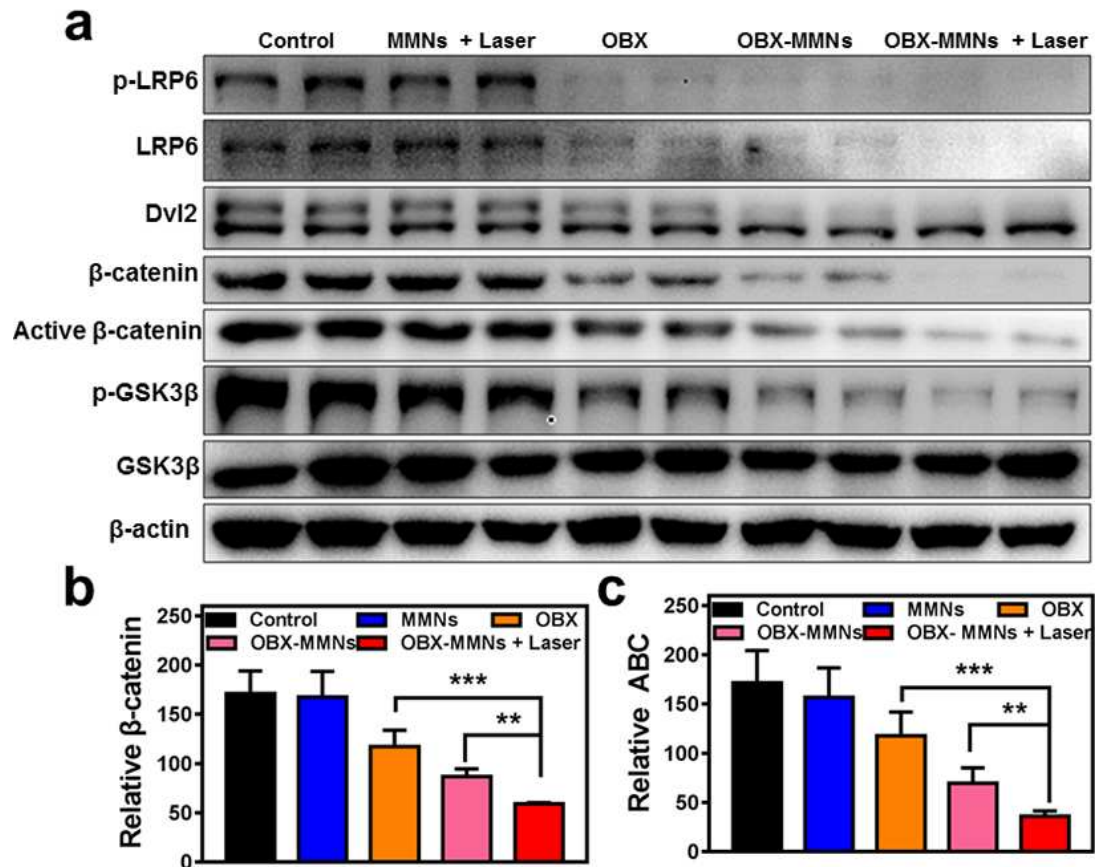


Fig. 7. OBX-MMNs inhibits the Wnt/ β -catenin signaling pathway *in vivo*.

(a) Phosphorylated LRP6 (Ser1490), total LRP6, DVL2, phosphorylated GSK3 β (Ser9), total GSK3 β , active β -catenin, and total β -catenin in MDA-MB-231 cells incubated with free OBX or OBX-MMNs without or with an 808 nm laser (5 min, 1.0 W cm⁻²) were detected by immunoblotting. Among them, in the DVL band, upper band represents phosphorylated DVL2. (b) The corresponding expression levels of total β -catenin and c) active β -catenin (ABC) in MDA-MB-231 cells incubated with free OBX or OBX-MMNs without or with an 808 nm laser (5 min, 1.0 W cm⁻²). All data are expressed as mean \pm SD (n = 5). NS: not significant, ** $P < 0.01$, *** $P < 0.001$.

Conclusions

In summary, OBX loaded melanin coated magnetic nanoparticles (OBX-MMNs) as pH/laser dual-stimuli responsive nanotheranostics for drug release and mild hyperthermia enhanced OBX-induced suppression of the

Wnt/ β -catenin signaling pathway. The as-prepared OBX-MMNs had excellent drug loading capability, photothermal stability and biocompatibility. Whole experiments verified that mild hyperthermia could dramatically enhance drug accumulation in tumor cells/tissues. Using laser as an exogenous stimulus to promote drug release and tumor uptake allows temporal and spatial precise control of therapeutic effects, and significantly decreases the systemic toxicity of chemotherapy drugs. Under the guidance of MR and PA dual-modal imaging, tumors treated with OBX-MMNs plus laser irradiation were completely eliminated with combined photothermal-chemo therapy. These results indicate that OBX-MMNs have great potential for cancer theranostics. In essence, our design strategy may open up a new way for OBX-mediated Wnt signaling suppression.

Materials and Methods

Reagents. Melanin was obtained from Sigma-Aldrich. OBX was obtained from Selleck. Iron (II) sulfate heptahydrate ($\text{FeSO}_4 \cdot 7\text{H}_2\text{O}$) was obtained from JK Chemical. Iron (III) chloride hexahydrate ($\text{FeCl}_3 \cdot 6\text{H}_2\text{O}$) was obtained from Mecklin. Methyl thiazolyl tetrazolium (MTT) was purchased from Sigma-Aldrich.

Synthesis of melanin coated magnetic nanoparticles (MMNs)

Biomimetic synthesis method was used to prepare MMNs through the co-precipitation of melanin with Fe^{3+} and Fe^{2+} ions (molar ratio 2:1) under nitrogen protection and alkaline conditions. Firstly, $\text{FeCl}_3 \cdot 6\text{H}_2\text{O}$ (0.9 mM) and $\text{FeSO}_4 \cdot 7\text{H}_2\text{O}$ (0.45 mM) were co-dissolved in the three-neck flask with 10 mL deionized water. Then the system was stirred vigorously at 80°C under N_2 protection for 10 min. Afterwards, 4 mL melanin ammonia (2.5 mg mL^{-1} , 1.5 M $\text{NH}_3 \cdot \text{H}_2\text{O}$) solution was immediately added to the flask, and kept stirring for 30 min. MMNs were separated by centrifugation at 10000 rpm for 15 minutes and

washed three times with deionized water.

Characterization of MMNs

Transmission electron microscopy (TEM) images were measured on a Tecnai TF30 (FEI, Hillsboro, OR). UV-Vis absorption spectra were taken on a Cary 60 UV-vis spectrophotometer (Agilent Technologies, Santa Clara, CA, USA). T2-weighted images of MMNs were measured by Magnetom Trio Tim 3.0 T (Siemens). PA images of the MMNs with different concentrations were captured on a Vevo 2100 LAZR system (VisualSonics).

Preparation of OBX-MMNs

OBX was dissolved in dimethyl sulfoxide (DMSO), and then added to MMNs solution (1 mg mL^{-1}). The mixture was sonicated for 5 min and then incubated for 12 h in a shaker (darkness, 40°C , 100 rpm). The product was then purified by centrifugation (8000 rpm, 10 min) for further use.

***In Vitro* Photothermal Property**

To detect the photothermal capability of OBX-MMNs, 200 μL OBX-MMNs of different concentrations (i.e. 30, 60, 120 and 240 nM) in Eppendorf tubes were exposed to an 808 nm laser (1 W cm^{-2} , 5 min). An infrared thermal camera (SC300, Arlington) was used to record the temperature changes.

Drug Loading and Release

OBX-MMNs were dissolved in 15% ethanol solution (500 μL) at pH 7.4 or 6.0 and shaken at 37°C (100 rpm). At the corresponding time points, OBX-MMNs were centrifuged by using ultrafiltration tube (Cut-off molecular weight: 300KDa) to collect the supernatant. The amount of OBX in the supernatant was calculated by UV-vis spectrometer using an established absorbance curve at 540 nm. The loading efficiency (LE) = (initial amount of feeding drugs - free drugs)/ (amount of OBX-MMNs). To measure the NIR-triggered drug

release, the solutions were exposed to NIR laser illumination for 5 min (808 nm, 1.0 W cm^{-2}) at the corresponding time points.

***In Vitro* Cell Experiments**

The cytotoxicity, cellular uptake and chemotherapeutic effect of OBX-MMNs were investigated in MDA-MB-231 and MDA-MB-468 cells. Tumor cells were seeded into 96-well plates at a density of 5×10^3 cells per well. After 24 h incubation, the samples were added and incubated for 24 h at the same condition. Then the standard MTT assays were performed to assess cell viability. To evaluate the influence of NIR illumination to the cellular uptake, MDA-MB-231 and MDA-MB-468 cells were seeded into 12-well plates. After 24 h incubation, the free OBX and OBX-MMNs groups (equivalent OBX dose: 1000 nM) were treated with/without an 808 nm laser (5 min, 1.0 W cm^{-2}). After irradiation, the cells were incubated for 1 h before replaced with fresh cell medium. The cellular uptake of OBX-MMNs was determined by confocal imaging and flow cytometer. To exert chemotherapy, MDA-MB-231 and MDA-MB-468 cells were seeded into 96-well plates and incubated with free OBX, MMNs and OBX-MMNs for 1 h, followed by exposure to an 808 nm laser with (5 min, 1.0 W cm^{-2}), and then incubation for up to 4 hours. Then the cell medium was replaced with the fresh medium and incubated for 20 h. The relative cell viability was detected by the standard MTT assay.

Lentivirus preparation and infection

To generate Bcl2 and β -catenin knockdown cells, oligonucleotides were inserted into pLKO.1 vector by AgeI/EcoRI digestion. The sequences of oligonucleotides are as follows: shcontrol-sense, 5'-CCGGTTCTCCGAACGTGTCACGTCTCGAGACGTGACACGTTCCGGAGATTTTTG-3'; shcontrol-antisense, 5'-AATTCAAAAATTCTCCGAACGTGTCACGTCTCGAGACGTGACACGTTCCGGAGAA-3'; shBcl2-1-sense,

5'-CCGGGTGATGAAGTACATCCATTATCTCGAGATAATGGATGTACTTCATC
 ACTTTTTG-3'; shBcl2-1-antisense,
 5'-AATTCAAAAAGTGATGAAGTACATCCATTATCTCGAGATAATGGATGTAC
 TTCATCAC-3'; shBcl2-2-sense,
 5'-CCGGCCGGGAGATAGTGATGAAGTACTCGAGTACTTCATCACTATCTCC
 CGGTTTTTG-3'; shBcl2-2-antisense,
 5'-AATTCAAAAACCGGGAGATAGTGATGAAGTACTCGAGTACTTCATCACT
 ATCTCCCGG-3'; sh β -catenin-1-sense,
 5'-CCGGGCTTGGAATGAGACTGCTGATCTCGAGATCAGCAGTCTCATTCC
 AAGCTTTTTG-3'; sh β -catenin-1-antisense,
 5'-AATTCAAAAAGCTTGGAATGAGACTGCTGATCTCGAGATCAGCAGTCTC
 ATTCCAAGC-3'; sh β -catenin-2-sense,
 5'-CCGGCAGATGGTGTCTGCTATTGTACTCGAGTACAATAGCAGACACCAT
 CTGTTTTTG-3'; sh β -catenin-2-antisense,
 5'-AATTCAAAAACAGATGGTGTCTGCTATTGTACTCGAGTACAATAGCAGA
 CACCATCTG-3'. The cloned pLKO.1 plasmid was transfected into HEK293T
 cells with psPAX2 and PMD2.G. The cells were infected with lentivirus and
 selected with 2 μ g/mL puromycin.

RNA isolation and Real-time PCR analyses

Total RNA was extracted by RNAiso Plus according to the manufacturer's
 instructions (TaKaRa). First strand cDNA was synthesized by the Primescript
 RT Reagent Kit according to the manufacturer's instructions (TaKaRa). Then
 prepared cDNA was subjected to the real-time PCR analysis using ABI Prism
 7300 Real-Time PCR System with Eastep qPCR Master Mix and primer
 mixtures. The primer sequences are as follows: cyclin D1-sense:
 5'-AATGACCCCGCACGATTTTC-3'; cyclin D1-antisense:
 5'-TCAGGTTTCAGGCCTTGAC-3'; LEF1-sense:
 5'-AGGAACATCCCCACACTGAC-3'; LEF1-antisense:

5'-AGGTCTTTTTGGCTCCTGCT-3'; fibronectin-sense:
 5'-ACCTACGGATGACTCGTGCTTT-3'; fibronectin-antisense,
 5'-TTCAGACATTCGTTCCCACTCA-3'; GAPDH-sense:
 5'-CCAGAACATCATCCCTGCCTCTACT-3'; GAPDH-antisense,
 5'-GGTTTTTCTAGACGGCAGGTCAGGT-3'. The comparative Ct method was used to analyze relative expression of genes.

Immunoblot Analysis

Protein samples were extracted from cells or tumor tissues using RIPA lysis buffer, followed by sonication. Western blotting was performed with phospho-LRP6 (Ser1490) (2568, CST), LRP6 (2560, CST), DVL2 (3216, CST), -phospho-GSK3 β (Ser9) (9322, CST), GSK3 β (9315, CST), cleaved caspase-3 (AB3623, Merck Millipor), nonphospho (active) β -catenin (8814, CST), β -catenin (sc-7963, Santa Cruz) and β -actin (HC-201, TransGen Biotech) antibodies.

Animal Model Study

Animal experiments were carried out in accordance with the protocol approved by the Animal Research Management Committee of Shenzhen University. For the Wnt1-driven mouse mammary tumor model, MMTV-Wnt1 transgenic mice were obtained from Jackson Laboratories. After breast tumors reached ~ 500 mm³, MMTV-Wnt1 mice were sacrificed and tumor fragments were implanted s.c. into BALB/c nude mice. When the tumor reached ~ 50 mm³, the mice were randomly divided into 5 groups (n = 5 per group): (a) saline group; (b) MMNs + laser group; (c) free OBX group; (d) OBX-MMNs group; (e) OBX-MMNs+ laser group. 200 μ L of OBX, OBX-MMNs or saline were *i.v.* injected every 3 days. 24 h after each injection, the tumor of mice in group (b) and (e) were exposed to an 808 nm laser (20 min, 1.0 W cm⁻²). Subsequently, tumor size and body weight were measured using a vernier calliper every 4 days after the

treatments. Tumor volume was calculated by the formula: $V = \text{Width}^2 \times \text{length}/2$.

***In Vivo* MRI**

The *in vivo* MRI was measured on Magnetom Trio Tim 3.0 T (Siemens). The mice were *i.v.* injected with OBX-MMNs (5 mg/kg, 200 μL) when the tumor size reached $\sim 50 \text{ mm}^3$. 24 h later, the tumor sites were irradiated with an 808 nm laser (20 min, 1.0 W cm^{-2}). MRI was performed at 4 h, 24 h after irradiation and immediately after laser irradiation. The conditions of MRI remained unchanged throughout the experiment. Signal strength was measured with an Image J software.

***In vivo* Photoacoustic and Photothermal Imaging**

The mice were *i.v.* injected with OBX-MMNs (5 mg/kg, 200 μL) when the tumor size reached $\sim 50 \text{ mm}^3$. 24 h later, the tumor sites were irradiated with an 808 nm laser (20 min, 1.0 W cm^{-2}). PAI was performed at 4 h, 24 h after irradiation and immediately after laser irradiation. The conditions of PAI remain unchanged throughout the experiment. PA imaging was accomplished by a Vevo 2100 LAZR system. PTT imaging was accomplished by an infrared thermal imager.

Histological Analysis

Five groups of tumors were collected at 18th day after treatment. Analysis was performed using hematoxylin & eosin (H&E) staining and immunohistochemistry. IHC was performed by using Ki-67 (12202, CST), β -catenin (8480, CST) and nonphospho (active) β -catenin (8814, CST) antibodies.

Acknowledgments

This work is financially supported by the National Natural Science Foundation of China (51703132, 51573096), the Basic Research Program of Shenzhen (JCYJ20160422091238319), the National Key Research and Development Program (2018YFA0704003), the Guangdong Province Natural Science Foundation of Major Basic Research and Cultivation Project (2018B030308003), and the Fok Ying-Tong Education Foundation for Young Teachers in the Higher Education Institutions of China (161032). We thank Instrumental Analysis Center of Shenzhen University (Lihu Campus).

Journal Pre-proof

References

- [1] R. Nusse, H. Clevers, Wnt/ β -catenin signaling, disease, and emerging therapeutic modalities, *Cell* 169(6) (2017) 985-999.
- [2] J.N. Anastas, R.T. Moon, Wnt signalling pathways as therapeutic targets in cancer, *Nat. Rev. Cancer* 13(1) (2013) 11-26.
- [3] H. Clevers, K.M. Loh, R. Nusse, An integral program for tissue renewal and regeneration: Wnt signaling and stem cell control, *Science* 346(6205) (2014) 1248012-1248028.
- [4] Z. Wang, B. Li, L. Zhou, S. Yu, Z. Su, J. Song, Q. Sun, O. Sha, X. Wang, W. Jiang, Prodigiosin inhibits Wnt/ β -catenin signaling and exerts anticancer activity in breast cancer cells, *P. Natl. Acad. Sci. USA* 113(46) (2017) 13150-13155.
- [5] P. Ordóñez-Morán, C. Dafflon, M. Imajo, E. Nishida, J. Huelsken, HOXA5 counteracts stem cell traits by inhibiting wnt signaling in colorectal cancer, *Cancer Cell* 28(6) (2015) 815-829.
- [6] P. Ordóñez-Morán, C. Dafflon, M. Imajo, E. Nishida, J. Huelsken, Bone metastasis of prostate cancer can be therapeutically targeted at the TBX2-Wnt signaling axis, *Cancer Res.* 77(6) (2017) 497-513.
- [7] A. Ambrosone, V. Marchesano, S. Carregal-Romero, D. Intartaglia, W.J. Parak, C. Tortiglione, Control of Wnt/beta-catenin signaling pathway in vivo via light responsive capsules, *Acs Nano* 10(4) (2016) 4828-4834.
- [8] H. Clevers, R. Nusse, Wnt/ β -catenin signaling and disease, *Cell* 149(6) (2012) 1192-1205.
- [9] N. Takebe, L. Miele, S.P. Ivy, Targeting Notch, Hedgehog, and Wnt pathways in cancer stem cells: clinical update, *Nat. Rev. Clin. Oncol.* 12(8) (2015) 445-464.
- [10] M. Masuda, M. Sawa, T. Yamada, Therapeutic targets in the Wnt signaling pathway: Feasibility of targeting TNIK in colorectal cancer, *Pharmacol. Therapeut.* 156 (2015) 1-9.
- [11] J. Waaler, O. Machon, L. Tumova, H. Dinh, V. Korinek, S.R. Wilson, J.E. Paulsen, N.M. Pedersen, T.J. Eide, O. Machonova, A novel tankyrase inhibitor decreases canonical Wnt signaling in colon carcinoma cells and reduces tumor growth in conditional APC mutant mice, *Cancer Res.* 72(11) (2012) 2822-2832.
- [12] S.M. Huang, Y.M. Mishina, S. Liu, A. Cheung, F. Stegmeier, G.A. Michaud, O. Charlat, E. Wiellette, Y. Zhang, S. Wiessner, Tankyrase inhibition stabilizes axin and antagonizes Wnt signalling, *Nature* 461(7264) (2016) 614-620.
- [13] D. Lu, M.Y. Choi, J. Yu, J.E. Castro, T.J. Kipps, D.A. Carson, Salinomycin inhibits Wnt signaling and selectively induces apoptosis in chronic lymphocytic leukemia cells, *P. Natl. Acad. Sci. USA* 108(32) (2011) 13253-13257.
- [14] P.-F. Cui, W.-R. Zhuang, X. Hu, L. Xing, R.-Y. Yu, J.-B. Qiao, Y.-J. He, F. Li, D. Ling, H.-L. Jiang, A new strategy for hydrophobic drug delivery using a hydrophilic polymer equipped with stacking units, *Chem. Commun.* 54(59) (2018) 8218-8221.
- [15] T. Liu, C. Wang, X. Gu, H. Gong, L. Cheng, X.Z. Shi, L.Z. Feng, B.Q. Sun, Z. Liu, Drug delivery with PEGylated MoS₂ nano-sheets for combined photothermal and chemotherapy of cancer, *Adv. Mater.* 26(21) (2014) 3433-3440.
- [16] P. Huang, P. Rong, A. Jin, X. Yan, M.G. Zhang, J. Lin, H. Hu, Z. Wang, X. Yue, W. Li, G. Niu, W. Zeng, W. Wang, K. Zhou, X. Chen, Dye-loaded ferritin nanocages for multimodal imaging and photothermal therapy, *Adv. Mater.* 26(37) (2014) 6401-6408.
- [17] J. Fang, H. Nakamura, H. Maeda, The EPR effect: Unique features of tumor blood vessels

- for drug delivery, factors involved, and limitations and augmentation of the effect ☆, *Adv. Drug Deliver. Rev.* 63(3) (2011) 136-151.
- [18] D. Peer, J.M. Karp, S. Hong, O.C. Farokhzad, R. Margalit, R. Langer, Nanocarriers as an emerging platform for cancer therapy, *Nat. Nanotechnol.* 2(12) (2007) 751-760.
- [19] L.C. Bai, X. Wang, S.B. Tang, Y.H. Kang, J.H. Wang, Y. Yu, Z.K. Zhou, C. Ma, X. Zhang, J. Jiang, P.K. Chu, X.F. Yu, Black phosphorus/platinum heterostructure: a highly efficient photocatalyst for solar-driven chemical reactions, *Adv. Mater.* 30(40) (2018) e1803641.
- [20] L. Chen, Y. Ji, X. Hu, C. Cui, H. Liu, Y. Tang, B. Qi, Y. Niu, X. Hu, A. Yu, Cationic poly-L-lysine-encapsulated melanin nanoparticles as efficient photoacoustic agents targeting to glycosaminoglycans for the early diagnosis of articular cartilage degeneration in osteoarthritis, *Nanoscale* 10 (28)(2018) 13471-13484.
- [21] R.P. Zhang, Q.L. Fan, M. Yang, K. Cheng, X.M. Lu, L. Zhang, W. Huang, Z. Cheng, Engineering melanin nanoparticles as an efficient drug-delivery system for imaging-guided chemotherapy, *Adv. Mater.* 27(34) (2015) 5063-5069.
- [22] S. Wang, P. Huang, X. Chen, Hierarchical targeting strategy for enhanced tumor tissue accumulation/retention and cellular internalization, *Adv. Mater.* 28(34) (2016) 7340-7364.
- [23] S. Wang, P. Huang, X. Chen, Stimuli-responsive programmed specific targeting in nanomedicine, *ACS Nano* 10(3) (2016) 2991-3004.
- [24] K. Yang, S. Zhang, G. Zhang, X. Sun, S.T. Lee, Z. Liu, Graphene in mice: ultrahigh in vivo tumor uptake and efficient photothermal therapy, *Nano Lett.* 10(9) (2010) 3318-3323.
- [25] N.S. Gandhi, R.K. Tekade, M.B. Chougule, Nanocarrier mediated delivery of siRNA/miRNA in combination with chemotherapeutic agents for cancer therapy: Current progress and advances, *J. Control Release* 194 (2014) 238-256.
- [26] W. Zhou, T. Pan, H. Cui, Z. Zhao, P.K. Chu, X.F. Yu, Black phosphorus: Bioactive nanomaterials with inherent and selective chemotherapeutic effects, *Angew. Chem. Int. Ed. Engl.* 58(3) (2018) 769-774.
- [27] Z. Zha, Z. Deng, Y. Li, C. Li, J. Wang, S. Wang, E. Qu, Z. Dai, Biocompatible polypyrrole nanoparticles as a novel organic photoacoustic contrast agent for deep tissue imaging, *Nanoscale* 5(10) (2013) 4462-4467.
- [28] S. Wang, J. Lin, Z. Wang, Z. Zhou, R. Bai, N. Lu, Y. Liu, X. Fu, O. Jacobson, W. Fan, Core-satellite polydopamine-gadolinium-metallofullerene nanotheranostics for multimodal imaging guided combination cancer therapy, *Adv. Mater.* 29(35) (2017) 1701013-1701021.
- [29] W. Tao, N. Kong, X. Ji, Y. Zhang, A. Sharma, J. Ouyang, B. Qi, J. Wang, N. Xie, C. Kang, H. Zhang, O.C. Farokhzad, J.S. Kim, Emerging two-dimensional monoelemental materials (Xenes) for biomedical applications, *Chem. Soc. Rev.* 48(11) (2019) 2891-2912.
- [30] X. Ji, Y. Kang, J. Ouyang, Y. Chen, D. Artzi, X. Zeng, Y. Xiao, C. Feng, B. Qi, N.Y. Kim, P.E. Saw, N. Kong, O.C. Farokhzad, W. Tao, Synthesis of ultrathin biotite nanosheets as an intelligent theranostic platform for combination cancer therapy, *Adv. Sci.* 6(19) (2019) 1901211.
- [31] N. Lu, P. Huang, W. Fan, Z. Wang, Y. Liu, S. Wang, G. Zhang, J. Hu, W. Liu, G. Niu, R.D. Leapman, G. Lu, X. Chen, Tri-stimuli-responsive biodegradable theranostics for mild hyperthermia enhanced chemotherapy, *Biomaterials* 126 (2017) 39-48.
- [32] D.K. Kirui, C. Celia, R. Molinaro, S.S. Bansal, D. Cosco, M. Fresta, H. Shen, M. Ferrari, Mild hyperthermia enhances transport of liposomal gemcitabine and improves in vivo therapeutic response, *Adv. healthc. mater.* 4(7) (2015) 1092-1103.

- [33] S. Wang, J. Weng, X. Fu, J. Lin, W. Fan, N. Lu, J. Qu, S. Chen, T. Wang, P. Huang, Black phosphorus nanosheets for mild hyperthermia-enhanced chemotherapy and chemo-photothermal combination therapy, *Nanotheranostics* 1(2) (2017) 208-216.
- [34] S.J. Madsen, E.C. Shih, Q. Peng, C. Christie, T. Krasieva, H. Hirschberg, Photothermal enhancement of chemotherapy mediated by gold-silica nanoshell-loaded macrophages: in vitro squamous cell carcinoma study, *Journal of biomedical optics* 21(1) (2016) 18004-18009.
- [35] D. Chen, C. Wang, F. Jiang, Z. Liu, C. Shu, L.J. Wan, In vitro and in vivo photothermally enhanced chemotherapy by single-walled carbon nanohorns as a drug delivery system, *J. Mater. Chem. B* 2(29) (2014) 4726-4732.
- [36] Y. He, T. Day, T. Zhang, H. Liu, X. Shi, L. Chen, G.J. Snyder, High thermoelectric performance in non-toxic earth-abundant copper sulfide, *Adv. Mater.* 26(23) (2014) 3974-3978.
- [37] P. Huang, P. Rong, J. Lin, W. Li, X. Yan, M.G. Zhang, L. Nie, G. Niu, J. Lu, W. Wang, Triphase interface synthesis of plasmonic gold bellflowers as near-infrared light mediated acoustic and thermal theranostics, *J. Am. Chem. Soc.* 136(23) (2014) 8307-8313.
- [38] Q. Zou, M. Abbas, L. Zhao, S. Li, G. Shen, X. Yan, Biological photothermal nanodots based on self-assembly of peptide-porphyrin conjugates for antitumor therapy, *J. Am. Chem. Soc.* 139(5) (2017) 1921-1927.
- [39] C. Ruan, L. Liu, Y. Lu, Y. Zhang, X. He, X. Chen, Y. Zhang, Q. Chen, Q. Guo, T. Sun, Substance P-modified human serum albumin nanoparticles loaded with paclitaxel for targeted therapy of glioma, *Acta. Pharm. Sin. B* 8(1) (2018) 85-96.
- [40] J. Lin, M. Wang, H. Hu, X. Yang, B. Wen, Z. Wang, O. Jacobson, J. Song, G. Zhang, G. Niu, Multimodal imaging guided cancer phototherapy by versatile biomimetic theranostics with UV and γ - irradiation protection, *Adv. Mater.* 28(17) (2016) 3273-3279.
- [41] L. Zhang, D. Sheng, D. Wang, Y. Yao, K. Yang, Z. Wang, L. Deng, Y. Chen, Bioinspired multifunctional melanin-mased nanoliposome for photoacoustic/magnetic resonance imaging-guided efficient photothermal ablation of cancer, *Theranostics* 8(6) (2018) 1591-1606.
- [42] F. Gong, L. Cheng, N. Yang, Q. Jin, L. Tian, M. Wang, Y. Li, Z. Liu, Bimetallic oxide nmoox nanorods for in vivo photoacoustic imaging of GSH and tumor-specific photothermal therapy, *Nano Lett.* 18(9) (2018) 6037-6044.
- [43] Q. Fan, K. Cheng, X. Hu, X. Ma, R. Zhang, M. Yang, X. Lu, L. Xing, W. Huang, S.S. Gambhir, Transferring biomarker into molecular probe: melanin nanoparticle as a naturally active platform for multimodality imaging, *J. Am. Chem. Soc.* 136(43) (2014) 15185-15194.
- [44] T. Yang, H. Ke, Q. Wang, Y. Tang, Y. Deng, H. Yang, X. Yang, P. Yang, D. Ling, C. Chen, Bifunctional tellurium nanodots for photo-induced synergistic cancer therapy, *Acs Nano* 11(10) (2017) 10012-10024.
- [45] X. Hu, J. Sun, F. Li, R. Li, J. Wu, J. He, N. Wang, J. Liu, S. Wang, F. Zhou, Renal-clearable hollow bismuth subcarbonate nanotubes for tumor targeted CT imaging and chemoradiotherapy, *Nano Lett.* 18(2) (2018) 1196-1204.
- [46] J. Lin, X. Chen, P. Huang, Graphene-based nanomaterials for bioimaging, *Adv. drug. deliver. rev.* 105 (2016) 242-254.
- [47] W. Tao, J. Wang, W.J. Parak, O.C. Farokhzad, J. Shi, Nanobuffering of pH-responsive polymers: A known but sometimes overlooked phenomenon and its biological applications, *ACS Nano* 13(5) (2019) 4876-4882.
- [48] M. Konopleva, J. Watt, R. Contractor, T. Tsao, D. Harris, Z. Estrov, W. Bornmann, H.

Kantarjian, J. Viallet, I. Samudio, M. Andreeff, Mechanisms of antileukemic activity of the novel Bcl-2 homology domain-3 mimetic GX15-070 (obatoclax), *Cancer Res.* 68(9) (2008) 3413-3420.

Journal Pre-proof

AUTHOR DECLARATION TEMPLATE

We the undersigned declare that this manuscript is original, has not been published before and is not currently being considered for publication elsewhere.

We would like to draw the attention of the Editor to the following publications of one or more of us that refer to aspects of the manuscript presently being submitted. Where relevant copies of such publications are attached. [CAN BE DELETED IF NOT RELEVANT]

We wish to draw the attention of the Editor to the following facts which may be considered as potential conflicts of interest and to significant financial contributions to this work. [OR]
We wish to confirm that there are no known conflicts of interest associated with this publication and there has been no significant financial support for this work that could have influenced its outcome.

We confirm that the manuscript has been read and approved by all named authors and that there are no other persons who satisfied the criteria for authorship but are not listed. We further confirm that the order of authors listed in the manuscript has been approved by all of us.

We confirm that we have given due consideration to the protection of intellectual property associated with this work and that there are no impediments to publication, including the timing of publication, with respect to intellectual property. In so doing we confirm that we have followed the regulations of our institutions concerning intellectual property.

We further confirm that any aspect of the work covered in this manuscript that has involved either experimental animals or human patients has been conducted with the ethical approval of all relevant bodies and that such approvals are acknowledged within the manuscript. [CAN BE DELETED IF NOT RELEVANT]

We understand that the Corresponding Author is the sole contact for the Editorial process (including Editorial Manager and direct communications with the office). He/she is responsible for communicating with the other authors about progress, submissions of revisions and final approval of proofs. We confirm that we have provided a current, correct email address which is accessible by the Corresponding Author and which has been configured to accept email from biomaterials@elsevier.com.

Signed by all authors as follows:

[LIST AUTHORS AND DATED SIGNATURES ALONGSIDE]

Tao Feng 2019-01-27

zhongxuan wang 2019-01-27

Liang Zhou 2019-01-27

Chunxiao Li 2019-01-27

Yifan Zhang 2019-01-27

Jiny 2019.01.29

Peng Huang 2019.1.29

Pesheng Lu 2019.01.27